Optimization of Slow Pyrolysis Process for Avocado peel and Cashew Nutshell Biochar Production: Physicochemical Properties and Stability for Carbon Sequestration

Atchara Chaiya[1,2], Ackapon Morgkhad[2], Apichaya Kemudorn[2], Chutithanyakan Siri[2] and Penwarat Panphattharachai[3, *]

[1] *Research and Development Unit for Agricultural Materials and Bio-Energy Properties, Rajamangala University of Technology Lanna, Chang Phueak, Mueang, Chiang Mai, 50300, Thailand*
[2] *Agricultural and Biological Engineering, Department of Mechanical Engineering, Rajamangala University of Technology Lanna, Chang Phueak, Mueang, Chiang Mai, 50300, Thailand*
[3] *Interdisciplinary and Technology College, Rajamangala University of Technology Lanna, Papong, Doisaket, Chiang mai, 50220, Thailand*

***Corresponding Author E-mail:** penwarat_s@rmutl.ac.th

Received: Jan 15, 2026; **Revised:** Mar 12, 2026; **Accepted:** Mar 16, 2026

Abstract

This study examined the slow pyrolysis of avocado peel (AP) and cashew nutshell (CNS) to produce biochar for adsorption, solid fuel, and carbon sequestration. Experiments were conducted at 400–600°C with residence times of 30–120 min, with process optimization via Response Surface Methodology (RSM). A central finding was a "physicochemical decoupling" effect, whereby conditions maximizing yield and adsorption capacity differ fundamentally from those required for carbon stability and energy densification. RSM models predicted maximum yield for both feedstocks at 400°C and 30 min, while peak iodine adsorption was achieved at 600°C — at 30 min for AP (530.19 mg/g) and 120 min for CNS (552.95 mg/g). SEM and elemental analyses confirmed that higher temperatures promoted well-developed porous networks and elevated carbon content, with Higher Heating Value (HHV) reaching 26.82 MJ/kg for AP and 32.20 MJ/kg for CNS, comparable to commercial biomass fuel benchmarks. Notably, CNS biochar at 600°C and 120 min achieved an O/C ratio of 0.055, classifying it as IBI Class 1 with a predicted carbon sequestration half-life exceeding 1,000 years. These results establish a condition-selection framework: 400°C for adsorbent production and 600°C for solid fuel and long-term carbon sequestration.

Keywords: Biochar, Slow pyrolysis, Carbon sequestration, Avocado peel, Cashew nutshell

1. Introduction

Thailand's status as a global agricultural hub ensures a continuous supply of diverse produce; however, shifting global consumption patterns towards health-conscious diets have significantly altered the agricultural landscape. Crops such as avocado and cashew nuts have witnessed a surge in global demand due to their high nutritional value and abundance of bioactive compounds [1–2]. While this popularity drives economic growth, it inevitably results in a corresponding increase in specific lignocellulos biomass wastes, accounting for approximately 21–31% (peel and stone combined) [3] and 70–75% [2] of the fresh fruit weight for Avocado peel and cashew nutshells, respectively. Conventional disposal methods, such as open burning or natural decomposition, not only represent a dissipation of valuable resources but also contribute significantly to greenhouse gas emissions. To address these challenges, the biochar system framework demonstrates a circular approach where agricultural waste is valorized via slow pyrolysis into bioenergy and stable carbonaceous materials [4] in alignment with the Paris Agreement's goals for carbon neutrality by 2050 [5].

From a materials engineering perspective, these biowastes exhibit a profound structural heterogeneity that fundamentally governs their pyrolytic behavior. avocado peel (AP) is characterized by a fibrous matrix with a relatively high holocellulose content [1], which facilitates rapid devolatilization and depolymerization during the initial stages of pyrolysis. In contrast, cashew nutshell (CNS) possesses a complex, extremely hard honeycomb structure with a significantly higher lignin density, often saturated with phenolic-rich cashew nutshell liquid (CNSL) [2]. This divergence in lignocellulosic profiles implies that AP and CNS will undergo distinct thermochemical pathways; while cellulose-rich AP is prone to rapid thermal fragmentation, the lignin-dense and phenolic-rich CNS is expected to exhibit higher thermal recalcitrance, providing a more robust carbon skeleton that influences the final skeletal density and mechanical strength of the biochar [6].

The mechanism of carbonization involves complex thermochemical reactions, including the cleavage of chemical bonds and the subsequent rearrangement of carbon atoms into stable polycyclic aromatic structures [7]. Crucially, process parameters such as temperature and residence time directly dictate the physicochemical evolution of the biochar. While temperature governs the thermodynamic equilibrium of bond cleavage, residence time influences the extent of secondary reactions and the liberation of volatile organic compounds, which are essential for surface area development and the formation of specific

functional groups [8]. These structural transformations directly enhance the material's surface reactivity and charge density [9], parameters that are critical for evaluating the performance of biochar in advanced engineering applications.

Beyond its physical properties, the application of biochar serves as a long-term carbon sequestration strategy, effectively locking carbon in a stable form and mitigating climate change impacts [4–5],[10]. However, a direct comparison of the thermal degradation pathways and carbon stability between avocado peel (fibrous/cellulose-dominant) and cashew nutshell (phenolic-oil/lignin-dominant) under identical pyrolysis conditions remains insufficiently explored. A significant research gap exists in understanding how the structural heterogeneity of these specific precursor influences "physicochemical decoupling." In this study, physicochemical decoupling refers to the phenomenon where the optimal pyrolysis conditions for enhancing physical properties (e.g., pore development for adsorption) diverge significantly from the conditions required to maximize chemical properties (e.g., aromatic condensation and energy densification).

Therefore, this research aims to investigate the influence of pyrolysis temperature and residence time on the yield, structural evolution, and physicochemical properties of biochar from these two distinct feedstocks. The study seeks to establish a fundamental correlation between the initial lignocellulosic composition and thermochemical behavior, providing a sustainable engineering solution for high-value waste management and carbon stability.

2. Materials and Methods

This section outlines the experimental design and analytical techniques employed to evaluate the thermochemical transformation of Avocado peel and cashew nutshell into engineered biochar. The methodology is structured to investigate the correlation between pyrolysis parameters and the resulting carbon stability and porous architecture. To provide essential context for interpreting pyrolysis behavior, the key physicochemical characteristics of the two feedstocks obtained from literature are summarized in **Table 1**.

2.1 Feedstock Preparation and Pretreatment

This study utilized two primary agricultural byproducts: avocado peel (AP) from the Booth 8 variety and cashew nutshell (CNS, *Anacardium occidentale* L.). Both feedstocks were collected directly from local agro-industrial processors in Chiang Mai, Thailand.

For avocado peel the samples were cleaned with deionized water, sliced into 2 × 3 cm segments, and dehydrated at 80°C for 24 h. In contrast, the pretreatment of cashew nutshell required a specific solid-liquid extraction unit operation to mitigate the pore-blocking effects of cashew nutshell liquid (CNSL). As illustrated in **Figure 1**, n-hexane was employed as the leaching agent due to its high selectivity for non-polar phenolic compounds (anacardic acid and cardanol) within the shell matrix [2].

The extraction was conducted at 50°C to enhance the diffusivity of the solvent into the complex honeycomb structure of the CNS, thereby facilitating the mass transfer of CNSL from the internal lignocellulosic matrix to the bulk solvent phase. This de-oiling step is critical to ensure that the subsequent carbonization allows for unobstructed volatile release and maximized micropore evolution. Prior to pyrolysis, both feedstocks were maintained at a moisture content of less than 5% (wet basis).

Table 1. Characteristics of the raw materials (AP and CNS) based on literature

Property	Avocado peel (AP), [11]	Cashew Nutshell (CNS), [12]
MC	55–65% (typical avocado by-products)	3.9% (reported for CNS prior to heating)
VM	High; early decomposition around 400 °C	81.4% High; strongly influenced by extractives
A	Moderate; K-, Mg-, Ca-rich	2.1% Low–moderate; minerals trapped in dense matrix
FC	Moderate; increases with T	16.5% Higher after CNSL removal
Structural features	Cellulose/hemicellulose-rich; soft matrix	Lignin-dense; CNSL (30–35%) present
Mineral content	Higher K and Mg; promotes alkaline pH	Ca and Mg embedded in compact shell; released at high T

*MC: Moisture content, VM: Volatile matter, A: Ash, FC: Fixed carbon

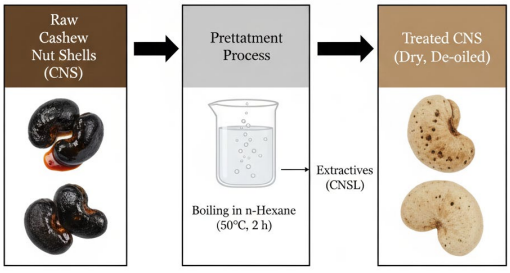

Figure 1 Schematic of the n-hexane extraction process for cashew nutshell liquid (CNSL) removal.

2.2 Biochar Production and Mass Balance Analysis

The transformation of biomass into biochar was executed through a thermochemical conversion process aimed at maximizing carbon stability and pore evolution. The slow pyrolysis was conducted in a

laboratory-scale fixed-bed reactor (with an internal volume of 15.12 L or dimensions of 280 mm × 150 mm × 360 mm) equipped with a PID controller (detailed in **Figure 2**).

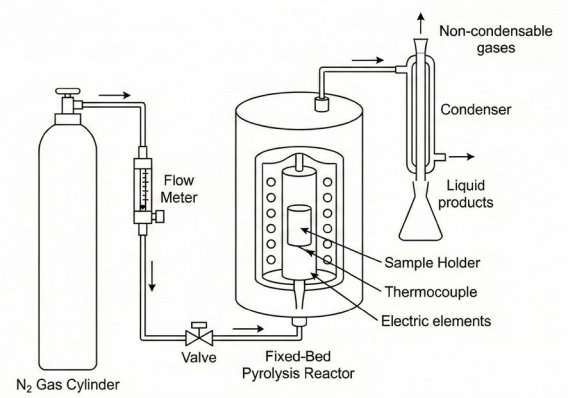

Figure 2 Schematic diagram of the laboratory-scale fixed-bed pyrolysis system

For each experimental run, 50 g of the prepared feedstock was loaded into the reactor chamber. An inert atmosphere was maintained by purging the system with nitrogen (N_2) gas at a constant flow rate of 5 L/min. The carbonization was conducted at peak temperatures of 400°C and 600°C, utilizing a constant heating rate of 10°C/min, with residence times varied at 30, 60, 90, and 120 min. During the thermal conversion, the evolved volatile gases were continuously routed through a condensation system, where the cooling water temperature was strictly maintained at 20°C to ensure efficient liquid condensation.

2.2.1 Rationale for Pyrolysis Conditions

The experimental parameters were calculated using the thermal degradation patterns of lignocellulosic biomass. The boundary temperatures of 400°C and 600°C were selected to represent two distinct carbonization regimes: 400°C marks the conclusion of the "active pyrolysis" zone, where hemicellulose and cellulose primarily decompose (200–400°C) to maximize mass yield and preserve surface functionality [13–14], whereas 600°C represents the “passive pyrolysis” or stabilization phase, characterized by extensive lignin degradation and aromatic condensation aimed at enhancing fix aimed at enhancing fixed carbon content and structural aromaticity [13–14].

An intermediate temperature of 500°C was deliberately included to bridge these two regimes. At this midpoint, secondary cracking of volatile organic compounds and substantial lignin degradation typically reach their zenith. In the Central Composite Design (CCD) architecture for process optimization, 500°C functions as the critical mathematical center necessary for assessing any non-linear impacts between the factorial extremes.

Furthermore, residence durations of 30 to 120 min were utilized to investigate the temporal progression of biochar properties. This range ensures sufficient time for comprehensive devolatilization at the minimum threshold (30 min) while enabling the identification of structural saturation and optimal energy efficiency over extended periods [15–16].

2.2.2 Mass Balance Analysis

To evaluate the process efficiency, the mass balance was accounted for based on the conservation of mass principle, as illustrated in **Figure 3**. The initial dry biomass ($W_{feedstock}$) was converted into three products: solid biochar (W_{char}), condensable bio-oil (W_{liquid}), and non-condensable syngas (W_{gas}). The biochar mass yield was specifically determined using Eq. (1):

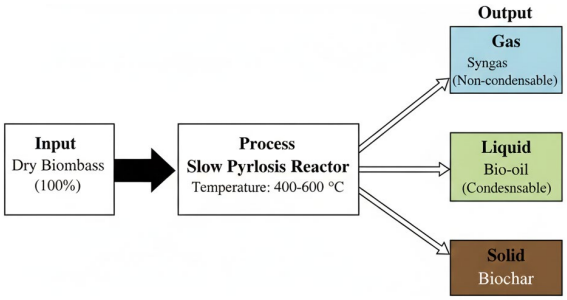

Figure 3 Mass balance diagram of the slow pyrolysis process

$$\text{Biochar Yield (\%)} = \left(\frac{W_{biochar}}{W_{feedstock}}\right) \times 100 \qquad (1)$$

where $W_{biochar}$ is the weight of the produced biochar (g) and $W_{feedstock}$ is the initial dry weight of the avocado peel or cashew nutshell (g).

2.3 Physicochemical Characterization

The physicochemical properties of the produced biochar were characterized to evaluate the structural transformations and chemical compositions resulting from the slow pyrolysis process. The analytical procedures were conducted as follows:

2.3.1 pH and Electrical Conductivity (EC)

The pH and electrical conductivity (EC) were assessed using a biochar-to-deionized water suspension at a 1:20 (w/v) ratio, adhering to established analytical techniques for biochar characterization [17]. The mixture was agitated with a magnetic stirrer for 1.5 hours and then allowed to equilibrate. The pH and EC values were then recorded using a calibrated pH/EC meter. These measurements were conducted on all samples to assess the progression of alkalinity and mineral salt concentration.

2.3.2 Surface Micropore Evolution (Iodine Number)

The iodine number, serving as a proxy for micropore development and surface area, was determined in accordance with the ASTM D4607-94 standard. Finely ground biochar was mixed with a 0.1 N standard iodine solution (N_2) and agitated to ensure equilibrium adsorption. The residual iodine in the filtrate was then titrated against a 0.1 N sodium thiosulfate ($Na_2S_2O_3$) standard solution (N_1) using a starch indicator. The iodine adsorption capacity was

calculated and reported in milligrams per gram (mg/g) using Eq. (2):

$$\text{Iodine Number (mg/g)} = \frac{\text{A - (DF} \times \text{B} \times \text{S)}}{\text{M}} \quad (2)$$

Where S is the volume of sodium thiosulfate used for titration (mL), M is the mass of the biochar sample (g), and DF represents the dilution factor. Constants A and B are derived from the normality of the iodine and sodium thiosulfate solutions, respectively.

2.3.3 Microstructural Analysis (SEM-EDS)

The surface morphology and pore structure were examined using Scanning Electron Microscopy (SEM, JEOL JSM-IT200). The biochar samples were mounted onto aluminum stubs using conductive carbon tape. The analysis was conducted under vacuum at an accelerating voltage of 10–15 kV. Images were captured at various magnifications to observe the development of honeycomb-like pore structures. Quantitative elemental analysis of surface carbon (C) and oxygen (O) was performed using Energy Dispersive Spectroscopy (EDS) integrated with the SEM system. To assess the degree of carbonization and deoxygenation, EDS analysis was specifically focused on samples produced at the maximum residence time (120 min) for each pyrolysis temperature.

2.3.4 Carbon Stability and Energy Potential Indices

To assess the degree of aromaticity and environmental persistence, the following stability indices were calculated based on EDS data**:**

1) *Atomic O/C Ratio:* This ratio indicates the degree of deoxygenation and the hydrophobicity of the biochar surface. It is a key predictor of the material's biological and chemical stability in various engineering applications, calculated using Eq. (3):

$$\text{Atomic O/C} = \frac{\text{O\%}/16.00}{\text{C\%}/12.01} \quad (3)$$

where O and C represent the weight percentages of oxygen and carbon from EDS, while 16.00 and 12.01 are their respective atomic weights.

2) *Atomic H/C Ratio:* This ratio serves as a primary indicator of the degree of aromaticity. A decrease in the H/C ratio reflects the structural transformation from aliphatic chains to stable polycyclic aromatic clusters due to intense dehydrogenation reactions. It was calculated using Eq. (4).

$$\text{Atomic H/C} = \frac{\text{H\%}/1.00}{\text{C\%}/12.01} \quad (4)$$

3) *Higher Heating Value (HHV):* The energy content was estimated using Dulong's formula as shown in Eq. (5):

$$\text{HHV(MJ/kg)} = 0.338(\text{C}) + 1.442(\text{H} - \frac{O}{8}) \quad (5)$$

where C and O are the weight percentage obtained from EDS analysis. Although the EDS analysis detected trace inorganic elements (e.g., K, Mg, and Ca), the reported elemental data focuses exclusively on carbon and oxygen. This targeted scope was established because the primary objective of this specific analysis was to evaluate carbon stability and aromatic condensation for biochar classification according to IBI standards. The broader influence of these inorganic minerals was instead assessed fundamentally through macroscopic parameters such as pH and electrical conductivity (EC). Furthermore, since EDS cannot reliably detect ultra-light elements, the hydrogen (H) content was estimated based on typical values for lignocellulosic biochar reported in the literature [10], assumed as 3.5% for 400°C and 2.0% for 600°C, respectively. Although this estimation introduces slight uncertainty in the absolute H/C values, it does not affect the comparative trends between AP and CNS biochar, as the thermodynamic mechanism of dehydrogenation at elevated temperatures is universal to both feedstocks. Therefore, the observed shifts toward increased aromaticity remain scientifically credible.

2.4 Statistical Data Analysis

All pyrolysis experiments and biochar characterizations were performed in triplicate to ensure reproducibility, with data reported as mean ± standard deviation. Statistical analysis was conducted using Minitab® 19 (Minitab Inc., USA).

To evaluate the influence of process parameters — pyrolysis temperature (X_1) and residence time (X_2) — on biochar properties (pH, EC, and Iodine Number), Response Surface Methodology (RSM) was employed. The experimental design was analyzed using Analysis of Variance (ANOVA) at a 95% confidence level ($p < 0.05$) to determine the statistical significance and the quality of the fit for the quadratic models. The relationship between the independent variables and the responses was expressed using the following second-order polynomial equation (Eq. (6)):

$$Y = \beta_0 + \sum \beta_i X_i + \sum \beta_{ii} X_i^2 + \sum \beta_{ij} X_i X_j \quad (6)$$

where Y is the predicted response, β_0 is the intercept, and β_i, β_{ii}, β_{ij} are the coefficients for linear, quadratic, and interaction effects, respectively. The adequacy of the models was verified using the coefficient of determination (R^2) and Lack-of-Fit tests.

Model adequacy and predictive capability were evaluated through ANOVA, R^2, adjusted R^2, predicted R^2, and lack-of-fit tests obtained from Minitab®. These internal validation metrics confirm the reliability of the RSM models without requiring additional external confirmatory experiments. Furthermore, Tukey's Honestly Significant Difference (HSD) test was applied for post-hoc multiple comparisons of the means.

3. Results and Discussion

3.1 Effect of Pyrolysis Conditions on pH and Electrical Conductivity

The pH and electrical conductivity (EC) of the produced biochar are critical indicators of their chemical stability and potential application in soil amendment. The experimental results, summarized in **Table 1**, demonstrate the variations in physicochemical properties across different temperatures and residence times. Statistical analysis reveals that while residence time showed minimal impact, pyrolysis temperature played a dominant role in governing these properties.

3.1.1 Alkalinity Evolution and De-acidification Mechanism

The pH values of the biochar showed unique temperature-dependent responses (**Table 2**). The pH of cashew nutshell (CNS) biochar consistently increased with elevated pyrolysis temperatures, but the avocado peel (AP) biochar attained its maximum pH at 500°C thereafter, decreasing at 600°C. In contrast to conventional biomass, which typically approaches neutrality, this biochar demonstrated pronounced alkaline characteristics even at lower pyrolysis temperatures, exhibiting pH values between 9.35 and 9.40 at 400°C and sustaining high alkalinity (>9.0) as the temperature increased to 600°C. The persistent high alkalinity indicates that the "deacidification" process, involving the thermal breakdown of acidic functional groups on the carbon surface, such as carboxyl (-COOH) and hydroxyl (-OH) groups, was predominantly accomplished even at 400°C [8]. The concurrent extraction of alkali salts from the organic matrix is essential. With increasing temperature, alkaline minerals like calcium carbonate ($CaCO_3$) and potassium carbonate (K_2CO_3), present in biomass ash, become more concentrated within the carbon matrix, therefore elevating or sustaining high pH levels [18].

A comparative investigation of feedstocks demonstrates varied behaviors influenced by their structural composition and ash characteristics. avocado peel (AP), as a byproduct of the fruit, possesses high concentrations of potassium (K) and magnesium (Mg) in its cellular structure, contributing to fruit development. Nonetheless, AP contains substantially more volatile alkali salts (such as potassium complexes). At 600°C, specific alkali minerals may begin to volatilize or convert into less soluble crystalline complexes, leading to the observed slight decrease in pH of AP biochar. The pH variation in cashew nutshell (CNS) biochar is affected by the presence of cashew nutshell liquid (CNSL), predominantly composed of anacardic acid. Despite the strong acidity of these phenolic lipids, the alkaline pH recorded at 400°C suggests that the thermal breakdown of these organic acids effectively neutralized their acidic properties.

Furthermore, the compact lignocellulosic matrix of CNS undergoes progressive structural degradation up to 600°C, releasing encapsulated alkaline earth metals (Ca and Mg) and thereby raising the pH considerably.

Table 2 Effect of pyrolysis temperature and residence time on pH and Electrical Conductivity (EC) of biochar derived from avocado peel (AP) and cashew nutshell (CNS).

Run	Temperature (°C)	Time (min)	AP biochar		CNS biochar	
			pH	EC (dS/cm)	pH	EC (dS/cm)
1	400	30	9.35 ± 0.09^{e}	0.03 ± 0.01^{g}	8.47 ± 0.07^{f}	0.29 ± 0.03^{k}
2	400	60	9.38 ± 0.11^{e}	0.04 ± 0.01^{g}	8.58 ± 0.08^{f}	$0.41 \pm 0.05^{j, k}$
3	400	90	9.34 ± 0.03^{e}	0.06 ± 0.01^{g}	$8.66 \pm 0.07^{e, f}$	$0.52 \pm 0.07^{i, j}$
4	400	120	9.40 ± 0.06^{e}	0.14 ± 0.01^{g}	9.14 ± 0.09^{d}	$0.68 \pm 0.02^{h, i}$
5	500	30	10.21 ± 0.04^{c}	0.23 ± 0.01^{g}	8.83 ± 0.01^{e}	$0.72 \pm 0.02^{g, h}$
6	500	60	10.52 ± 0.11^{a}	0.46 ± 0.07^{f}	9.07 ± 0.02^{d}	0.89 ± 0.01^{g}
7	500	90	$10.26 \pm 0.07^{b, c}$	$0.51 \pm 0.05^{e, f}$	9.09 ± 0.02^{d}	1.13 ± 0.06^{f}
8	500	120	$10.48 \pm 0.07^{a, b}$	$0.72 \pm 0.03^{d, e}$	$9.35 \pm 0.05^{b, c}$	1.64 ± 0.07^{e}
9	600	30	9.93 ± 0.10^{d}	0.88 ± 0.09^{d}	$9.23 \pm 0.02^{c, d}$	2.39 ± 0.10^{d}
10	600	60	9.89 ± 0.12^{d}	1.31 ± 0.02^{c}	$9.52 \pm 0.04^{a, b}$	3.59 ± 0.05^{c}
11	600	90	9.82 ± 0.04^{d}	1.59 ± 0.16^{b}	9.61 ± 0.10^{a}	4.32 ± 0.08^{b}
12	600	120	9.70 ± 0.05^{d}	2.16 ± 0.13^{a}	9.69 ± 0.13^{a}	5.64 ± 0.11^{a}

Note: Values are presented as mean ± standard deviation (n=3). Different superscript letters within the same column indicate significant differences ($p < 0.05$) according to Tukey's HSD test.

3.1.2 Electrical Conductivity and Ash Enrichment Effect

The electrical conductivity (EC) of the biochar exhibited a positive correlation with pyrolysis temperature, with the highest value observed at 600°C for both feedstocks (**Table 2**). This trend is governed by the "Ash Enrichment Effect." As the pyrolysis temperature increases, the organic mass (C, H, O, N) is progressively lost through volatilization, whereas the inorganic ionic minerals (K, Na, Ca, Mg) are non-volatile and remain within the carbon matrix. Consequently, while the total mass of the char

decreases, the concentration of these salts per unit weight increases, leading to higher EC values [19].

Regarding feedstock differences, AP biochar generally exhibited higher EC values or a faster rate of increase compared to CNS biochar under identical conditions. This can be attributed to the inherent nature of the biomass; the soft tissue structure of avocado peel contains vascular bundles rich in soluble salts required for nutrient transport. Conversely, CNS possesses a dense lignocellulosic structure (hard shell) where minerals may be fixed within a less soluble crystalline matrix or present in lower total ash quantities compared to fresh fruit peels. Thus, the release of conductive ions in CNS biochar is slightly lower than in AP biochar at comparable carbonization intensities.

3.2 Optimization of Biochar Production using RSM

3.2.1 Pyrolysis Behavior of Avocado peel (AP) Biochar

The Analysis of Variance (ANOVA) for avocado peel (AP) revealed that both temperature (X_1) and residence time (X_2) exerted highly significant negative effects ($p < 0.001$) on the biochar yield **(Table 3)**. This observation is consistent with the continuous downward slope of the response surface shown in **Figure 4**. Regarding the iodine number, the interaction effect between temperature and residence time (X_1X_2) was found to be the most influential factor ($p = 0.000$), suggesting that the development of the pore structure in AP biochar is not governed by a single independent variable but rather by a synergistic effect.

The response surface plot for the iodine number of AP exhibited a characteristic dome-shaped profile, indicating an optimal condition within the intermediate temperature range (500–550°C). This phenomenon can be attributed to the fact that while increasing temperatures facilitate the removal of volatile matter and initiate pore opening, excessive thermal treatment (600°C) may lead to ash fusion or the collapse of pore walls, subsequently diminishing absorption efficiency. The regression model for yield demonstrated a high R^2 value of 93.40% (**Table 3**), confirming its robust predictive capability for the carbonization of this feedstock as expressed in the mathematical model in **Table 4**.

3.2.2 Pyrolysis Behavior of Cashew Nutshell (CNS) Biochar

For cashew nutshell (CNS), the statistical models displayed exceptional precision, with the R^2 value for yield reaching 97.56% **(Table 5)**. The exceptionally high F-value for temperature (1139.53) underscores that thermal energy is the critical factor controlling the decomposition of this specific biomass. In terms of the iodine number, the quadratic term of temperature (X_1^2) was highly significant ($p = 0.000$), resulting in a more pronounced curvature in the response surface compared to the AP samples.

The behavior of CNS differed significantly from AP, as the iodine number showed a continuous upward trend up to the maximum studied temperature (600°C). This suggests that the lignocellulosic framework of CNS possesses superior thermal stability and requires higher activation energy to achieve peak pore development. Furthermore, the significantly lower yield of CNS compared to AP (less than 25%) is attributed to the rapid volatilization of the high oil and volatile organic content inherent in cashew nutshell during the carbonization process. The quantitative relationships for these responses are further detailed by the regression equations provided in **Table 4**.

3.2.3 Comparative Synthesis

A comparative analysis between the two feedstocks, based on the statistical parameters summarized in **Tables 3 and 5**, indicates that their response mechanisms to pyrolysis temperature and time are distinct, governed primarily by their initial chemical compositions:

1. Yield Efficiency: CNS is more temperature-sensitive than AP and yields a lower quantity of biochar due to substantial mass loss from the evaporation of volatile components.

2. Adsorptive Quality (Iodine Number): AP reaches pore development saturation earlier at moderate temperatures (500–550°C), whereas CNS requires higher thermal intensity (600°C) to maximize its adsorption performance.

3. Model Reliability: The mathematical models for CNS demonstrated a superior goodness-of-fit compared to AP for both quantity and quality responses. This indicates that the control parameters in the CNS biochar production process are well-defined and highly predictable within the experimental design space, as evidenced by the high R^2 values and significant model terms in **Table 4**.

The elevated R^2 values, significant ANOVA models, and satisfactory lack-of-fit tests derived from Minitab® validate the dependability and predictive efficacy of both the AP and CNS models. Therefore, the model-based optimization results reported in this study are statistically robust even without external validation experiments.

The AP models (**Table 3**) demonstrated strong reliability, as indicated by the high coefficient of determination ($R^2 = 93.40\%$ for yield and 74.55% for iodine number) and the non-significant lack-of-fit for yield. These statistical indicators confirm that the quadratic RSM model adequately explains the variability in AP biochar responses and possesses satisfactory predictive capability within the studied design space.

The CNS model (**Table 5**) is highly predictive, with high R^2 values (97.56% for yield and 88.18% for iodine number), significant ANOVA results, and acceptable lack-of-fit values. These measurements demonstrate that the RSM model delivers accurate predictions for CNS biochar generation without the need for external validation studies.

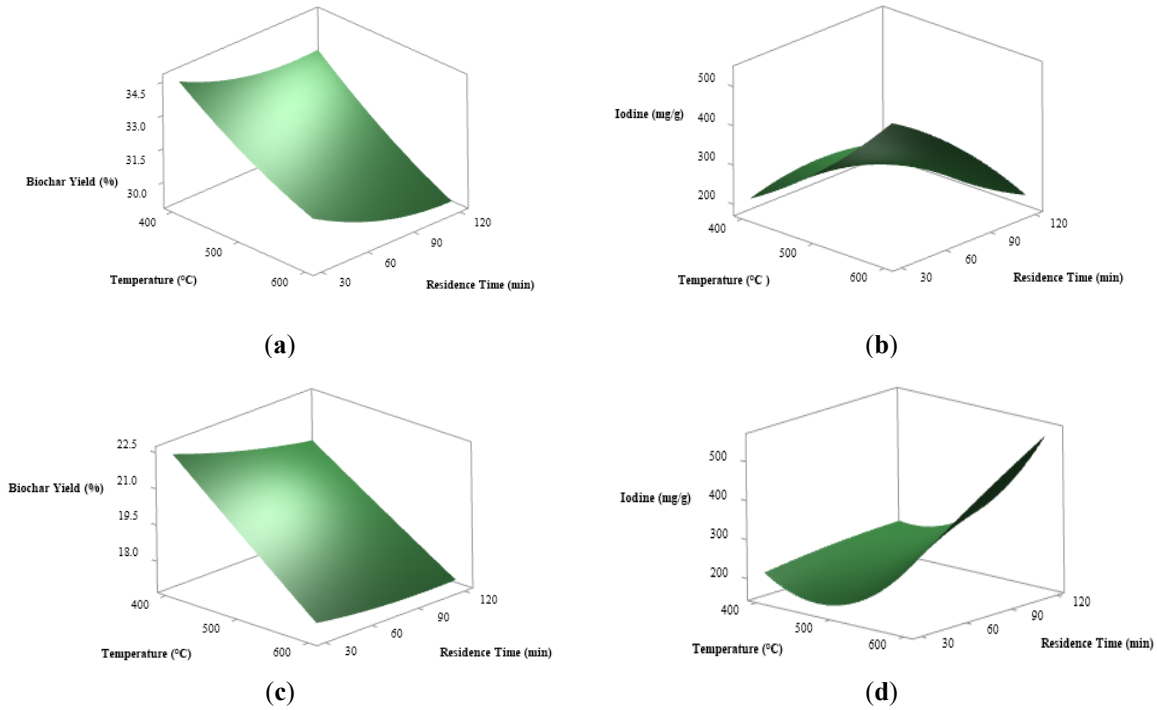

Figure 4 Response surface plots showing the effect of pyrolysis temperature and residence time on: (**a**) Biochar Yield of AP, (**b**) Iodine Number of AP, (**c**) Biochar Yield of CNS, and (**d**) Iodine Number of CNS.

Table 3 ANOVA for the Quadratic Models of Biochar Yield and Iodine Number (avocado peel - AP)

Source	DF	F-Value (Yield)	P-Value (Yield)	F-Value (Iodine)	P-Value (Iodine)
Model	5	84.93	0.000*	17.58	0.000*
- Temperature (X_1)	1	360.41	0.000*	34.73	0.000*
- Residence Time (X_2)	1	53.04	0.000*	29.43	0.000*
- X_1^2	1	2.94	0.097	1.23	0.276
- X_2^2	1	6.75	0.014*	1.35	0.255
- $X_1 \times X_2$	1	1.51	0.229	21.15	0.000*
Lack-of-Fit	6	0.72	0.637	25.32	0
R^2 (%)		93.40%		74.55%	

*Significant at $p<0.05$

Table 4 Final Regression Equations in Uncoded Units for Biochar Production

Material	Response (Y)	Regression Equation	R^2 (%)
AP	Yield	$Y = 49.36 - 0.0458X_1 - 0.0347X_2 + 0.000030X_1^2 + 0.000235X_2^2 - 0.000036X_1X_2$	93.40%
	Iodine	$Y = -84 - 0.40X_1 + 9.39X_2 + 0.00253X_1^2 - 0.0139X_2^2 - 0.01810X_1X_2$	74.55%
CNS	Yield	$Y = 34.69 - 0.0297X_1 - 0.0553X_2 + 0.000002X_1^2 + 0.000071X_2^2 + 0.000068X_1X_2$	97.56%
	Iodine	$Y = 2341 - 9.06X_1 - 3.78X_2 + 0.00925X_1^2 - 0.00292X_2^2 + 0.01130X_1X_2$	88.18%

Note: X_1 is Temperature (°C) and X_2 is Residence Time (min).

Table 5 ANOVA for the Quadratic Models of Biochar Yield and Iodine Number (cashew nutshell - CNS)

Source	DF	F-Value (Yield)	P-Value (Yield)	F-Value (Iodine)	P-Value (Iodine)
Model	5	239.43	0.000*	44.74	0.000*
- Temperature (X_1)	1	1139.53	0.000*	129.10	0.000*
- Residence Time (X_2)	1	44.08	0.000*	42.28	0.000*
- X_1^2	1	0.05	0.83	34.71	0.000*
- X_2^2	1	1.44	0.24	0.13	0.725
- $X_1 \times X_2$	1	12.05	0.002*	17.49	0.000*
Lack-of-Fit	6	2.06	0.096	4.84	0.002
R^2 (%)		97.56%		88.18%	

*Significant at $p<0.05$

The RSM-derived ideal pyrolysis parameters for yield and iodine number of AP and CNS biochar are shown in **Table 6**, along with values from related research in literature. In the case of AP biochar, the model predicted a maximum yield of 34.58% at 400°C and 30 min. Notably, peak adsorption performance (iodine number of 530.19 mg/g) was achieved under a markedly different condition — 600°C and 30 min— where sufficient thermal energy drives pore opening without extended exposure that risks structural collapse. A similar pattern emerged for CNS biochar: maximum yield (22.35%) was predicted at 400°C and 30 min, yet the iodine number continued to rise with increasing temperature and time, peaking at 552.95 mg/g under 600°C and 120 min, owing to the greater thermal resistance of its lignin-rich shell. The fact that yield and adsorption optima fell at different conditions for both materials is direct evidence of the physicochemical decoupling central to this work—no single set of process parameters can simultaneously optimize both properties. Compared with previous studies, the predicted yields of both biochar are within a comparable range to those reported in the literature, while the iodine numbers remain competitive, confirming the adsorption potential of the biochar produced under the identified optimum conditions.

Table 6 RSM-predicted optimum conditions for biochar yield and iodine number of AP and CNS biochar, with comparison to previous studies

Feedstock	Optimum Condition (Max Yield)	Predicted Yield (%)	Optimum Condition (Max Iodine No.)	Predicted Iodine No. (mg/g)	Reference
avocado peel (AP)	400°C – 30 min	34.58	600°C – 30 min	530.19	This study
cashew nutshell (CNS)	400°C – 30 min	22.35	600°C – 120 min	552.95	This study
avocado seed biochar	500°C – 20 min	34.00	–	–	[11]
cashew nutshell – heat-treated	300°C – 120 min	46.50	–	–	[12]

Note: Predicted values derived from RSM regression equations (Table 4). Optimum conditions determined by maximizing each response independently within the experimental domain (400–600°C; 30–120 min).

3.3 Surface Morphology (SEM Analysis)

Following the findings in Section 3.1, which indicated that temperature played a dominant role in physicochemical changes, and the RSM analysis in Section 3.2, which highlighted the complex behavior of iodine adsorption, biochar samples produced at a residence time of 120 minutes were selected for surface morphology examination. This selection was made to elucidate the microstructural mechanisms driving the statistical trends observed in the RSM models and to compare the structural evolution of avocado peel (AP) and cashew nutshell (CNS) at extreme temperature conditions (400°C and 600°C).

The SEM micrographs at ×2,000 magnification, presented in **Figure 5**, reveal a stark contrast in surface morphology driven by thermal variance, providing physical evidence for the adsorption behaviors reported earlier. At the lower pyrolysis temperature of 400°C (**Figures 5a and 5c**), the surfaces of both AP and CNS biochar appear relatively smooth and dense. Most pores remain small, undeveloped, and obscured by debris. This observation strongly correlates with the lower Iodine Numbers predicted by the RSM model at low temperatures for CNS. The presence of residual volatiles and tars clogging the pores restricts the diffusion of iodine molecules into the internal carbon matrix, thereby limiting adsorption capacity.

Conversely, at 600°C (**Figures 5b and 5d**), the surface structure underwent a significant transformation characterized by the emergence of numerous deep and interconnected pores. Specifically, the AP600 sample displayed a well-ordered, honeycomb-like structure with thinner pore walls. This highly porous morphology corroborates the high adsorption efficiency observed in the RSM optimization zone. The cleaning of pore channels allows for greater accessibility to active sites, directly supporting the high Iodine Number values obtained.

The observed morphology aligns with fundamental pyrolysis mechanisms and explains the physicochemical decoupling discussed in Section 3.3. The smooth and undeveloped surface at 400°C results from incomplete thermal decomposition. As explained by Lehmann and Joseph [4], at lower temperatures, high-molecular-weight hydrocarbons and tars partially remain and condense, causing pore blockage. This limited surface area not only explains the lower Electrical Conductivity (EC) due to poor water infiltration but also justifies the significant interaction effect (X_1X_2) found in the RSM analysis, where temperature increase is required to "unlock" these pores.

According to Basu [6], the formation of large, open pores at 600°C is attributed to intensified devolatilization. High thermal energy generates internal pressure that rigorously expels moisture and volatile matter from the cellulose and lignin matrix. For CNS specifically (**Figure 5d**), the rupture of its dense lignocellulosic shell at 600°C created new macro-channels, which visually confirms why the Iodine Number for CNS continued to rise significantly with temperature in the quadratic model (X_1^2), unlike the softer AP biomass which developed pores earlier.

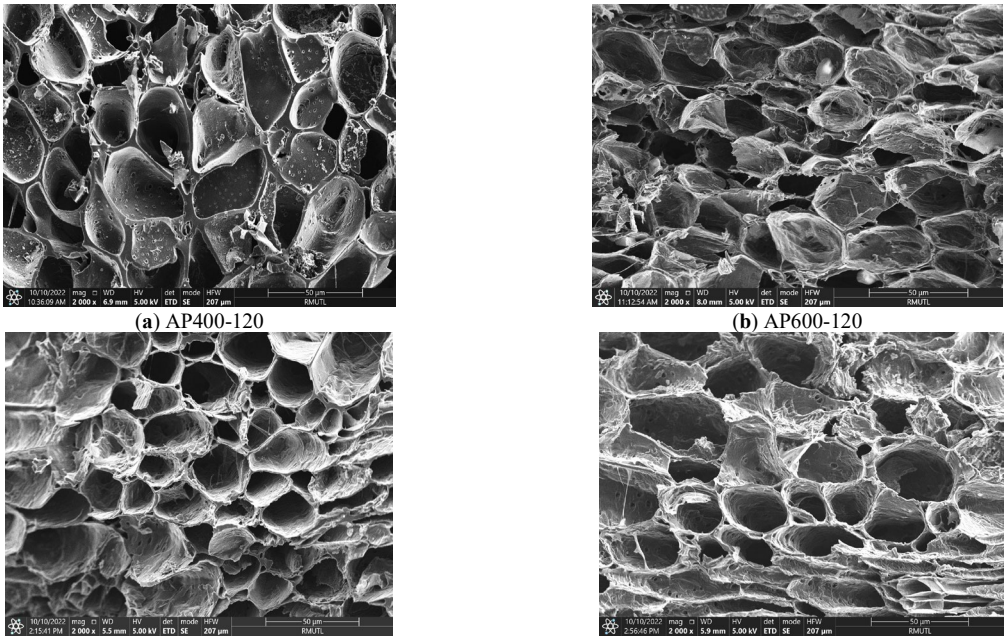

(**a**) AP400-120 (**b**) AP600-120

(**c**) CNS400-120 (**d**) CNS600-120

Figure 5 SEM micrographs (×2,000 magnification) illustrating the surface morphology of biochar produced at a residence time of 120 min: (**a**) avocado peel at 400°C, (**b**) avocado peel at 600°C, (**c**) cashew nutshell at 400°C, and (**d**) cashew nutshell at 600°C.

3.4 Chemical Stability and Carbon Sequestration Potential

In addition to physical properties, the elemental analysis presented in **Table 7** reveals profound changes in the molecular structure of the biochar, particularly at the 120-minute residence time. These chemical alterations further substantiate the material quality in terms of energy densification and long-term structural stability.

The chemical transformation of avocado peel (AP) and cashew nutshell (CNS) during pyrolysis was observed by analyzing the changes in their atomic ratios. The elemental composition of raw biomass was sourced from known literature [1–2] to generate a baseline for the Van Krevelen analysis, as depicted in **Figure 6**. In this analytical context, the H/C ratio serves as an indicator of aromaticity and structural condensation, whereas the O/C ratio indicates surface hydrophilicity and long-term environmental stability.

At 600°C and a 120-minute residence time, the biochar's atomic H/C ratio dropped significantly to 0.42–0.48 (calculated on a molar basis), reflecting the development of a highly condensed aromatic structure. This reduction signifies extensive dehydrogenation, leading to the formation of stable polycyclic aromatic hydrocarbons (PAHs) and graphene-like sheets. As shown in the Van Krevelen diagram, the shift of data points from the upper-right toward the lower-left corner represents the coalification pathway. This significant shift is primarily driven by dehydration and decarboxylation reactions, which effectively remove oxygen and hydrogen from the biomass matrix, conferring chemical signatures similar to anthracite.

Most importantly, the carbon sequestration potential was validated through the International Biochar Initiative (IBI) standards. Both AP600 and CNS600 biochar achieved an atomic O/C ratio below the 0.2 threshold, with CNS600 reaching an exceptionally low value of 0.055 (while AP600-120 reached 0.15).

Table 7 Physicochemical properties, atomic ratios, and heating value of biochar produced at 120 min residence time compared to adsorption trends.

Sample	Iodine No. Trend	Atomic O/C	Atomic H/C*	HHV** (MJ/kg)	Stability Class (IBI)	Potential Application
AP400-120	193.153	0.204	0.574	26.050	Class 2	Soil Amendment & Nutrient Release
AP600-120	207.385	0.150	0.301	26.822	Class 1	Carbon Sequestration (Long-term)
CNS400-120	256.277	0.117	0.495	31.197	Class 1	Biofuel & Soil Conditioner
CNS600-120	560.355	0.055	0.264	32.201	Class 1	High-Permanence Carbon Storage

***** Calculated based on estimated hydrogen content derived from lignocellulosic biochar literature [18].

** Calculated using Dulong's formula.

Note: Stability classes are defined according to the International Biochar Initiative (IBI) guidelines based on the atomic O/C ratio: Class 1 (O/C < 0.2) represents highly stable biochar with a half-life > 1,000 years, suitable for carbon sequestration; Class 2 (0.2 < O/C < 0.6) represents moderately stable biochar suitable for soil amendment;

Class 3 (O/C > 0.6) represents unstable biochar mainly for fuel or immediate nutrient release.

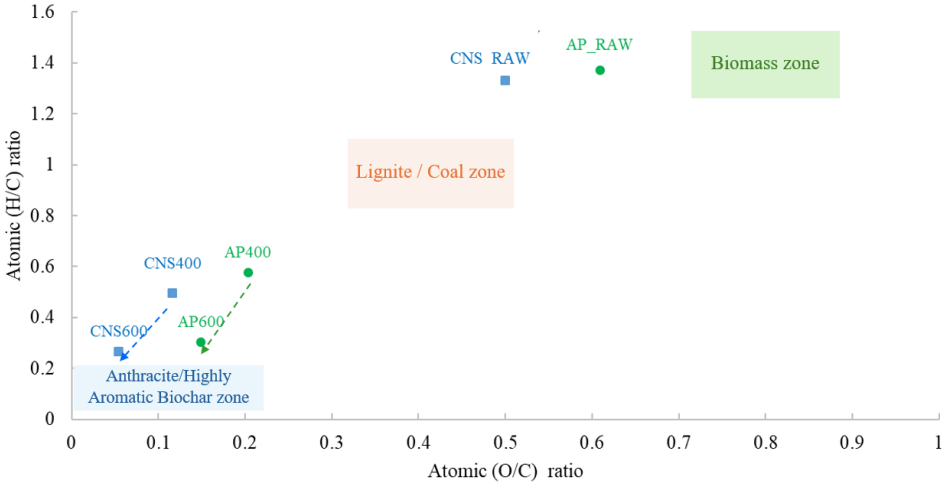

Figure 6 Van Krevelen diagram illustrates the elemental evolution and carbonization pathways of avocado peel (AP) and cashew nutshell (CNS) biochar. The arrows indicate the coalification trajectory from 400°C to 600°C. The shift of data points toward the "Anthracite" region (lower-left corner) signifies advanced dehydration and decarboxylation, resulting in high carbon stability and enhanced aromaticity.

This classifies the materials as Class 1 biochar, possessing high aromatic condensation and a predicted half-life exceeding 1,000 years in soil environments. Consistent with findings by Spokas [20] and Budai et al. [10], such a minimal O/C ratio demonstrates exceptional resistance to microbial and abiotic oxidation. This positioning within the highly stable region confirms a predicted carbon sequestration half-life in soil exceeding 1,000 years, making these biochar superior candidates for climate change mitigation. Based on the guidelines presented in **Table 7**, integrating this biochar into agricultural and environmental systems requires a clear distinction between their functional roles. In particular, a soil amendment is primarily associated with chemical and nutritional improvements (e.g., pH buffering and nutrient supply, which are appropriate for AP400), whereas a soil conditioner is associated with physical structural improvements (e.g., enhancing water retention and aeration through porous networks, which is a feature of highly stable biochar such as CNS600) (**Figure 7**). This functional divergence further underscores that physicochemical decoupling is directly governed by the pyrolysis temperature employed.

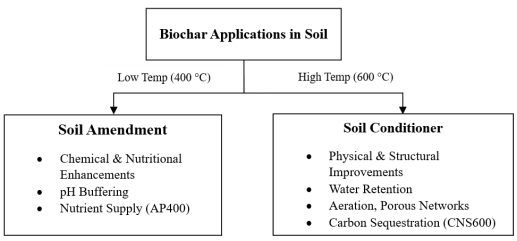

Figure 7 Conceptual framework of the physicochemical decoupling effect determining biochar applications: low-temperature soil amendment versus high-temperature soil conditioner.

Furthermore, the energy content of the biochar was evaluated through the Higher Heating Value (HHV). At the 120-minute residence time, a clear trend of energy densification was observed. The HHV reached its peak at 26.82 MJ/kg for AP600 and an impressive 32.20 MJ/kg for CNS600. This enhancement is attributed to the removal of low-energy volatile matter and the subsequent concentration of fixed carbon. Interestingly, a "physicochemical decoupling" effect was identified: while the iodine adsorption capacity of AP600 decreased due to the partial sintering and physical collapse of micropores at extended residence times, its HHV and carbon stability reached their maximum. This phenomenon demonstrates that although a 120-minute residence time may adversely affect the porous structure for adsorption purposes, it is the optimal condition for producing high-grade solid fuels and stable carbon sequestration agents.

4. Conclusion

This study optimized the slow pyrolysis of avocado peel (AP) and cashew nutshell (CNS) biochar production using RSM, revealing a significant physicochemical decoupling between adsorption performance and carbon stability. Reduced pyrolysis temperatures (~400°C) yielded greater biochar production and maintained porosity for adsorption purposes, whereas elevated temperatures (600°C) facilitated structural condensation, energy densification, and enhanced long-term carbon stability, essential for solid fuel and carbon sequestration applications.

Microstructural and chemical analysis demonstrated that heating conditions influence not only pore architecture, but also the elemental content and stability class of the resulting biochar. At 600°C for 120 min, both feedstocks produced biochar with a

strong alkaline character, well-developed porous networks, and HHV values of 26.82 MJ/kg (AP) and 32.20 MJ/kg (CNS), which are comparable to commercial biomass benchmarks, indicating their potential as value-added carbon materials in a circular economy framework.

In conclusion, this work presents a practical decision framework for selecting pyrolysis settings according to desired application: 400°C for adsorbent manufacture and 600°C with longer residence time for high-grade solid fuels and long-term carbon sequestration. The IBI Class 1 stability classification achieved by CNS biochar further highlights its potential contribution to climate change mitigation strategies. Future research should explore a comparative assessment of n-hexane de-oiling versus mechanical pressing as CNS pre-treatment methods, as such a comparison would be critical in evaluating the cost-effectiveness and scalability of the pre-treatment process for applications in industry.

5. Acknowledgments

The authors would like to express their sincere gratitude to the School of Renewable Energy, Maejo University, Chiang Mai, Thailand to providing the laboratory facilities and equipment essential for the pyrolysis experiments. We also extend our special appreciation to the Research Center for Materials and Manufacturing Processes, Faculty of Engineering, Rajamangala University of Technology Lanna, Chiang Mai, Thailand. for their technical support in surface morphology characterization using Scanning Electron Microscopy (SEM).

6. References

[1] M. C. García-Vargas, M. D. M. Contreras, I. Gómez-Cruz, J. M. Romero-García and E. Castro, "Avocado-Derived Biomass: Chemical Composition and Antioxidant Potential," *Proceedings*, vol.70, no. 1, 2021, Art. no. 100 doi: 10.3390/foods_2020-07750.

[2] K. W. Y. Chung, J. Blin, C. Lanvin, E. Martin, J. Valette and L. Van De Steene, "Pyrolysis of cashew nut shells— focus on extractives," *Journal of Analytical and Applied Pyrolysis*, vol. 179, 2024, Art. no. 106452, doi: 10.1016/j.jaap.2024.106452.

[3] M. C. García-Vargas, M. del Mar Contreras and E. Castro, "Avocado-derived biomass as a source of bioenergy and bioproducts," *Applied Sciences*, vol. 10, no. 22, 2020, Art. no. 8195, doi: 10.3390/app10228195

[4] J. Lehmann and S. Joseph, "Biochar for environmental management," in *Biochar for Environmental Management: Science, Technology and Implementation Science, Technology and Implementation*, 3rd ed. London, U.K.: Routledge, 2024, ch. 1, pp. 1–14.

[5] United Nations, "The Paris Agreement," United Nations Climate Change, 2015. [Online]. Available: https://unfccc.int/process-and-meetings/the-paris-agreement

[6] P. Basu, "Pyrolysis," *in Biomass Gasification, Pyrolysis and Torrefaction: Practical Design and Theory,* 3rd ed. London, U.K.: Academic Press, 2013, ch. 5, pp.155–187.

[7] K. Weber and P. Quicker, "Properties of biochar," *Fuel*, vol. 217, pp. 240–261, 2018, doi: 10.1016/j.fuel.2017.12.054.

[8] J. -H. Yuan, R. -K. Xu and H. Zhang, "The forms of alkalis in the biochar produced from crop residues at different temperatures," *Bioresource Technology*, vol. 102, no. 3, pp. 3488–3497, 2011, doi: 10.1016/j.biortech.2010.11.018.

[9] D. L. Sparks, "Sorption Phenomena on Soils," in *Environmental Soil Chemistry*, 2nd ed. Amsterdam, Netherlands: Academic Press, 2003, ch. 5, pp. 133–186

[10] A. Budai, A. R. Zimmerman, A. L. Cowie, J. B. W. Webber, B. P. Singh, B. Glaser, C. A. Masiello, D. Andersson, F. Shields, J. Lehmann, M. Camps Arbestain, M. Williams, S. Sohi and S. Joseph, "Biochar carbon stability test method: An assessment of methods to determine biochar carbon stability," International Biochar Initiative (IBI), 2013. [Online]. Available: https://biochar-international.org/wp-content/uploads/2018/04/IBI_Report_Biochar_Stability_Test_Method_Final.pdf

[11] A. Rahmat, H. Hidayat, L. P. Lestari, E. Elfarisna, I. Indriyani, M. Apriyanto, L. Nuraini, H. Hariadi and A. Mutolib, "Evaluation of the characteristics of avocado seed biochar at various pyrolysis temperatures for sustainable waste management," *Universal Journal of Agricultural Research*, vol. 12, no. 1, pp. 201–210, 2024, doi: 10.13189/ujar.2024.120120.

[12] B. S. Kadjo, M. K. Sako, K. A. Diango, A. Danlos, and C. Perilhon, "Characterization and optimization of the heat treatment of cashew nutshell to produce a biofuel with a high-energy value," *AIMS Energy*, vol. 12, no. 2, pp. 387–407, 2024, doi: 10.3934/energy.2024018.

[13] A. Tomczyk, Z. Sokołowska and P. Boguta, "Biochar physicochemical properties: pyrolysis temperature and feedstock kind effects," *Reviews in Environmental Science and Bio/Technology*, vol. 19, pp. 191–215, 2020, doi: 10.1007/s11157-020-09523-3.

[14] R. Chatterjee, B. Sajjadi, W.-Y. Chen, D. L. Mattern, N. Hammer, V. Raman and A. Dorris, "Effect of Pyrolysis Temperature on PhysicoChemical Properties and Acoustic-Based Amination of Biochar for Efficient CO2 Adsorption," *Frontiers in Energy Research*, vol. 8, 2020, Art. no. 85, doi: 10.3389/fenrg.2020.00085.

[15] Z. Wang, K. Liu, L. Xie, H. Zhu, S. Ji and X. Shu, "Effects of residence time on characteristics of biochars prepared via co-pyrolysis of sewage sludge and cotton stalks," *Journal of Analytical and Applied Pyrolysis*, vol. 142, 2019, Art. no. 104659, doi: 10.1016/j.jaap.2019.104659.

[16] S. You, Y. S. Ok, S. S. Chen, D. C. W. Tsang, E. E. Kwon, J. Lee and C. -H Wang, "A critical review on

sustainable biochar system through gasification: Energy and environmental applications," *Bioresource Technology*, vol. 246, pp. 242–253, 2017, doi: 10.1016/j.biortech.2017.06.177.

[17] M. T. Haraz, L. Bowtell and R. A. Al-Juboori, "Biochar Effects on Nutrients Retention and Release of Hydroponics Growth Media," *Journal of Agricultural Science*, vol. 12, no. 8, pp. 1–13, 2020, doi: 10.5539/jas.v12n8p1.

[18] B. Singh, B. P. Singh and A. L. Cowie, "Characterization and evaluation of biochars for their application as a soil amendment," *Australian Journal of Soil Research*, vol. 48, no. 7, pp. 516–525, 2010, doi: 10.1071/SR10058.

[19] M. K. Hossain, V. Strezov, K. Y. Chan, A. Ziolkowski and P. F. Nelson, "Influence of pyrolysis temperature on production and nutrient properties of wastewater sludge biochar," *Journal of Environmental Management*, vol. 92, no. 1, pp. 223–228, 2011, doi: 10.1016/j.jenvman.2010.09.008.

[20] K. A. Spokas, "Review of the stability of biochar in soils: predictability of O:C molar ratios," *Carbon Management*, vol. 1, no. 2, pp. 289–303, 2010, doi: 10.4155/cmt.10.32.